# Correlation between failure mechanism and rupture lifetime of 2D-C/SiC under stress oxidation condition based on acoustic emission pattern recognition

Peng Lv[1,2], Leijiang Yao[1], Xiaofei Ma[2], Gang An[2], Guodong Bai[3], Andy T. Augousti[4], Xiaoyan Tong[1]

*1. Laboratory of Science and Technology on UAV, Northwestern Polytechnical University, Xi'an 710065, China*

*2. Xi'an Institute of Space Radio Technology, Xi'an 710100, China*

*3. School of Aeronautics, Northwestern Polytechnical University, Xi'an 710072, China*

*4 Faculty of Science, Engineering and Computing, Kingston University London, SW15 3DW UK*

**Abstract**

Creep tests of 2D-C/SiC in a wet oxidizing atmosphere were implemented for six samples. The loading process was monitored by acoustic emission (AE). Principal component analysis and a fuzzy clustering algorithm were used to perform pattern recognition of the AE data. All of the AE events were divided into four clusters and labelled as matrix cracking, interfacial damage, fiber breakage and fiber-bundle breakage respectively, according to their physical origin. It was found C/SiC has very scattered rupture lifetimes even under the same test conditions, and the evolution of AE events corresponding to fiber failure is quite different. With increasing rupture lifetime, the AE energy of fiber-bundle breakage is higher, while the number of these events is less. Thus, it is concluded that local oxidation and damage development is the controlling failure mechanism for short-lived specimens and uniform oxidation and damage development is the controlling failure mechanism for long-lived specimens.

Keywords: ceramic matrix composites; stress oxidation; damage mechanism; acoustic emission; pattern recognition.

# 1. Introduction

Continuous carbon fiber reinforced silicon carbide matrix composites (C/SiC) exhibit excellent mechanical properties at elevated temperature and have been developed for aeronautic and aerospace applications [1,2]. In service, C/SiC is subject to complex coupling effects between thermal, stress and chemical reactions, and its damage evolution and failure mechanisms are of wide interest [3-6]. Generally, there is oxidation along with several kinds of microscopic fracture mechanisms involving stress oxidation of C/SiC in a wet oxidizing atmosphere, including matrix cracking, interface debonding, delamination and fiber breakage. Their evolution depends on the microscopic structure, especially defects in preparation, such as coating cracks, matrix cracks and porosities. Due to the random size and distribution of these defects, C/SiC usually shows a wide scatter in its performance, even under the same stress and environmental conditions.

In order to describe the failure process, researchers often rely on some physical information released from the internal changes in materials to describe the damage process, such as electrical resistance [7-9], mechanical parameters [10-12], thermal dissipation [13], acoustic emission (AE) [14-20] or their combinations [21-24]. AE, which is a phenomenon whereby transient elastic waves are generated by strain energy release, provides a passive method of monitoring the changes within a material [25,26]. Since one micro-fracture event will generate one AE wave and various fracture mechanisms will generate AE signals with different characteristics, it is believed that AE is a powerful means to characterize the damage evolution of

materials. Moreover, AE can be applied under conditions of elevated temperature using waveguides.

However, there are challenges in the application of AE in the study of the damage mechanisms of ceramic matrix composites (CMCs). One of the most important is that the complexity of the AE source itself, as well as the complex propagation and attenuation processes within the material, make it difficult to correlate AE events with microscopic fracture mechanisms. Researchers have tried to solve this problem with pattern recognition technology, mainly unsupervised cluster analysis [14, 27, 28]. The method has been used to analyze several kinds of CMCs and has been able to identify that AE signal grouping has a strong correlation with damage mechanisms [14, 27].

In the present paper, a fuzzy C-means (FCM) algorithm was used instead of the more common K-means algorithm to improve the effectiveness of cluster analysis of AE data from creep tests of C/SiC in a wet oxidizing atmosphere. The damage mechanisms and their evolution were characterized by AE cluster analysis. Combined with the AE data and fracture surface observation, the dominant controlling failure mechanism for C/SiC with different rupture lifetimes under particular stress oxidation conditions is proposed.

## 2. Experimental

### 2.1. Preparation of Specimens

Plain woven carbon fiber preforms with a fiber volume fraction of 40% were employed. A pyrolytic carbon (PyC) interface and SiC matrix were deposited via chemical vapor infiltration (CVI) processes. The precursors of PyC and SiC were

Propene ($C_3H_6$) and Methyltrichlorosilane (MTS, $CH_3SiCl_3$), respectively [29]. Then the fabricated C/SiC was machined into dog-bone shaped samples, as shown in Fig. 1. Finally, a chemical vapor deposition (CVD) process was used to deposit a SiC coating.
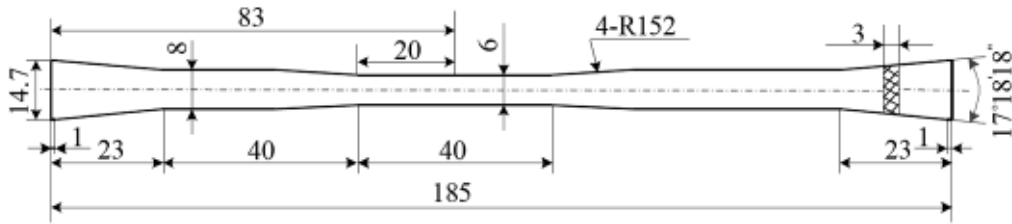


Fig. 1. Geometry of the creep test specimens.

*2.2. Creep Tests*

Tensile creep tests were performed on a servo-hydraulic test machine (Model INSTRON 8801) equipped with a resistance heating furnace. A schematic of the test equipment and specimen setup can be found elsewhere [30, 31]. The tensile stress applied was 140MPa and the temperature employed was 1300°C. The atmosphere in the furnace was maintained at 79% argon, 5% water vapor and 16% oxygen by mass flow controllers. Only the gauge parts of the specimens were kept in the hot zone. Specimens were held for several minutes at the test temperature prior to creep testing. Then they were loaded to the required tensile stress (140MPa) under a constant stress rate of 2.4MPa/s. To prevent oxidation of the fracture surface, the atmosphere was changed to pure argon immediately after the specimen broke. Six samples were tested and denoted by S1, S2, S3, S4, S5, and S6 in order of increasing rupture lifetime. Morphologies of the ruptured specimens were observed with a scanning electron microscope (Hitachi, TM4000PLUS).

*2.3. AE Monitoring*

AE signals were detected by two WD sensors (Physical Acoustic Corporation, PAC) clamped at both ends of the specimen. One sensor was used as the main recording sensor andthe other as a reference sensor. The reference sensor ensures that only signals originating from the middle of the sample will be recorded, thus rejecting common-mode noise. AE data was collected during the whole of the creep tests using a PCI-2 AE system (PAC), with a sampling rate of 1MSPS. AE signals were frequency filtered between 20kHz and 1.2MHz, pre-amplified by 40dB. An amplitude threshold of 40dB was set to obtain AE hits.

## 3. Pattern recognition techniques

AE signals generated by different microscopic fracture mechanisms have their special features. which can be described by a number of parameters (or descriptors) extracted from the AE waveforms, such as energy, average frequency, amplitude, rise time, duration, counts, etc. Pattern recognition is required to establish a mapping between AE signals and fracture mechanisms. Since no labelled data is available, an unsupervised methodology is used to perform the pattern cluster analysis. It involves the following steps: (a) feature selection or feature extraction, (b) clustering, (c) cluster validity analysis and (d) labelling the clusters. [14]

*3.1 Feature selection and extraction*

Dealing with the classification of AE waveforms, discrete features must be selected. To improve the accuracy of classification, it is desirable that the number of types of features is as small as possible. Principal Component Analysis (PCA) was used as a

feature extraction and selection method. PCA is a statistical method of decreasing the dimensionality of a signal, whereby the signal is transformed by an orthogonal transformation into a new random vector whose components are only related to components of the original signal via this transformation [32]. The selected principal components (PC) were the most representative eigenvectors, whose contributions were defined as corresponding collectively to more than 85% of the data set standard deviation.

*3.2 Fuzzy c-means clustering algorithm*

The fuzzy c-means (FCM) algorithm, developed by Dunn in 1973 [33] and improved by Bezdek in 1981 [34], is one of the most widely used fuzzy clustering algorithms. In classic or hard clustering approaches (e.g. K-means), an object is either definitely a member of a set or not, with its membership degree being 1 or 0, respectively. In soft or fuzzy membership theory, an object can belong to a cluster at any degree of membership ranging from 0 to 1 [35]. Fuzzy clustering may refer to either fuzzy data analysis or precise data analysis using fuzzy techniques. FCM is the most widely used fuzzy clustering algorithm in practice [36]. Compared with K-means algorithm, FCM provides greater versatility in processing complex data. The FCM clustering algorithm aims to minimize the following objective function

$$J_m(U,V,X) = \sum_{i=1}^{c} \sum_{k=1}^{n} u_{ik}^m \parallel x_k - v_i \parallel^2 \tag{1}$$

Where $X=(x_k \in R^n,\ k = 1,2,\ldots,n)$ is the set of data, $x_k$ is represented by an n-dimensional feature vector, the matrix $V = (v_1,\ v_2,\ldots,\ v_c)$ is an n-by-c matrix consisting of $c$ cluster centers, $U=(u_{ik})$ is a $c$-by-$n$ matrix representing the degree of

membership of samples belonging to the fuzzy subset, $c$ is the number of clusters, $m$ is the weighting exponent (fuzzy index) which determines the amount of fuzziness of the resulting partition and takes a value in the range $[1, \infty]$. The FCM algorithm minimizes the objective function by iteratively updating cluster prototypes $V$ and membership degree $U$.

$$v_i = \frac{\sum_{k=1}^{n} u_{ik}^m x_k}{\sum_{k=1}^{n} u_{ik}^m}, \ 1 \leqslant i \leqslant c \tag{2}$$

$$u_{ik} = \left[ \sum_{j=1}^{c} \left( \frac{\|x_k - v_i\|}{\|x_k - v_j\|} \right)^{\frac{2}{m-1}} \right]^{-1}, \ 1 \leqslant i \leqslant c, \ 1 \leqslant k \leqslant n \tag{3}$$

Where $u_{ik}$ is the degree of membership of $x_k$ in the cluster $i$ with a numerical value in $[0, 1]$.

The clustering result is the degree of membership of each data point to the clustering center, which is expressed by a numerical value. By repeatedly evaluating Eqs. (2) and (3), the objective function $J_m$ gradually tends to its minimum value [37].

*3.3 Clustering validity*

The Xie and Beni (XB) index [38], the Dunn index [33] and the Davies Bouldin (DB) index [39] were selected to check the validity of the clustering results. The number of classes was determined when the optimal index values were obtained.

**4. Results and discussion**

*4.1 Creep test results*

The creep curves of the six samples are shown in Fig. 2. The creep process includes two stages, namely the transient creep stage (t<100 s) and the stationary, or steady,

creep stage (t>100s). The creep strain increases rapidly and the creep rate decreases gradually in the first stage, corresponding to the loading process. The creep strain increases very slowly in the steady stage, with almost constant creep rate. The steady creep rate is defined to be the slope of the steady stage. The rupture lifetimes and steady creep rates of the six samples are listed in Table 1. Even under the same test conditions, the rupture lifetime varies significantly, due to the complex coupling mechanism of stress and oxidation involved in the failure process of C/SiC under these test condition, as well as the presence of random defects within the materials. It can be seen from Fig. 3 that there is no consistent relationship between creep rate and lifetime. Thus, it seems to be impossible to explain the variation in the rupture lifetime only by the apparent creep strain data.

Table 1 Creep test results

| Sample No. | S1 | S2 | S3 | S4 | S5 | S6 |
|---|---|---|---|---|---|---|
| Rupture lifetime (min) | 23 | 51 | 77 | 98 | 165 | 166 |
| Steady creep rate ($s^{-1}$) | $3.962 \times 10^{-8}$ | $1.799 \times 10^{-6}$ | $3.489 \times 10^{-7}$ | $4.078 \times 10^{-7}$ | $1.775 \times 10^{-7}$ | $1.841 \times 10^{-7}$ |
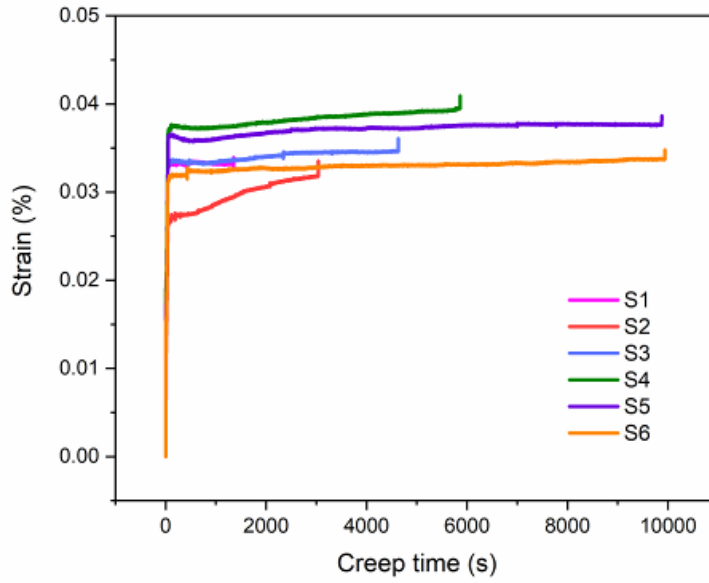
Fig. 2. Creep strain curves
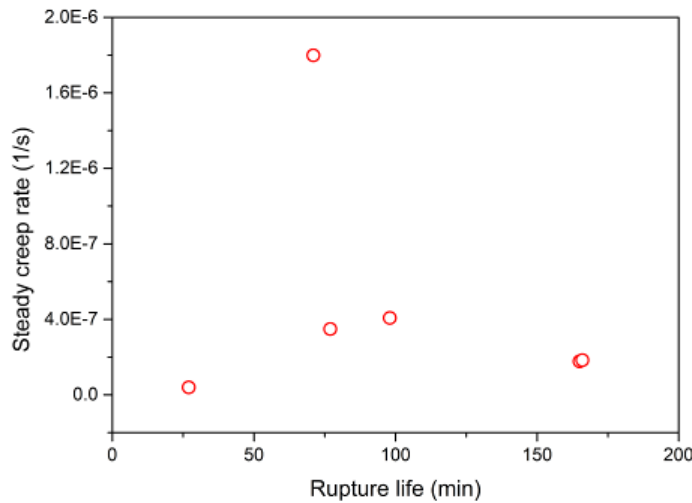


Fig.3. Steady creep rate of samples with various rupture lifetimes

*4.2 Unsupervised clustering of AE events in the creep tests*

AE data collected from the creep tests of six samples were identified using PCA and FCM cluster analysis. Fig.4 shows the XB index, Dunn index and DB index calculated from the clustering results of S3 obtained by taking a range of clusters between 2-10. It is found that the number of clusters c=4 gives the best result,

indicating that the AE events can be divided into four classes. Fig.5 shows the results of fuzzy c-means clustering with different principal components of S3, including the combinations of principal component 1 and principal component 2, 3, 4 and 5. It is seen that the AE data of each class is reasonably well separated.

In Fig.5, there is a single outlier point. This is assigned to Class A. The existence of this AE event has a significant influence on the failure mechanism, which will be discussed later.

*4.3 Cluster labelling*

It is reasonable to believe that each class represents one kind of fracture mechanism, and the center of each class reflects the basic physical foundation of corresponding fracture mechanism. Therefore, by analyzing the features of each cluster center, the resulting four clusters can be assigned to appropriate microscopic fracture mechanisms. The values of the primary descriptors of the four cluster centers are listed in Table 2.
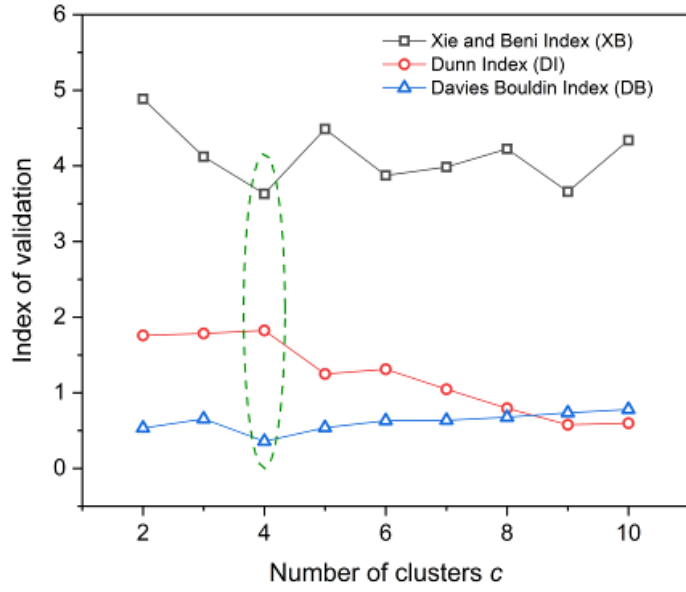
Fig. 4. Index values obtained from different number of clusters (S3)
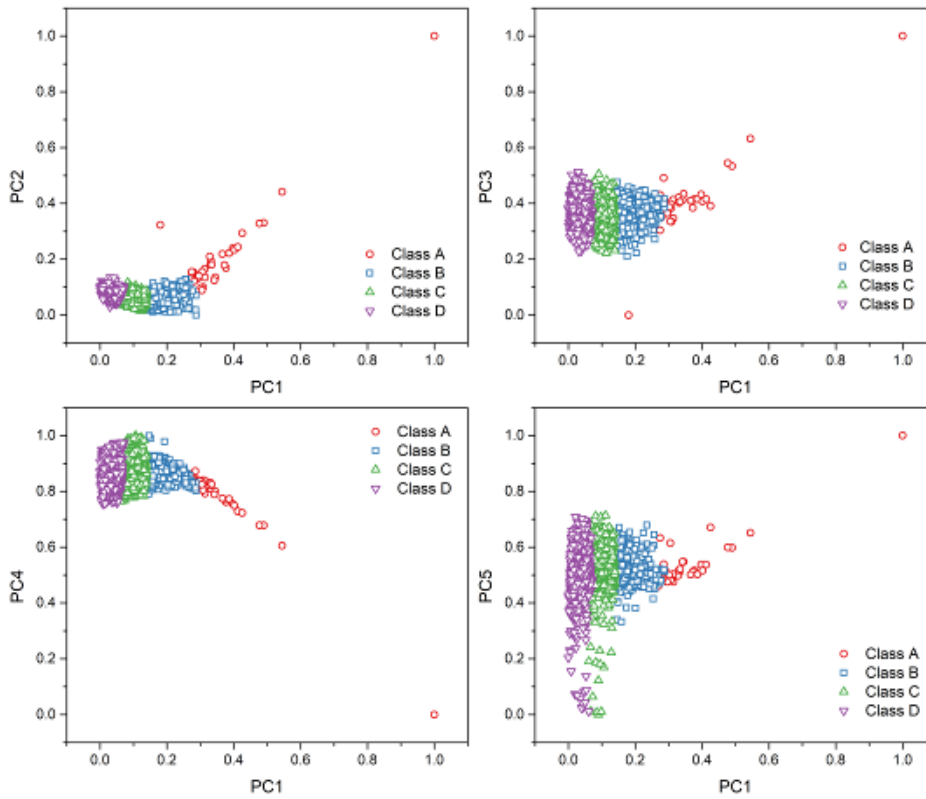


Fig. 5. PCA visualization of the fuzzy c-means clustering (S3)

Table 2 AE features of the cluster centers

| Sample No. | Class | Average Frequency (kHz) | Energy (10μVs) | Rise time (μs) | Onset time (s) |
|------------|-------|-------------------------|----------------|----------------|----------------|

| | | | | | |
|---|---|---|---|---|---|
| | A | 278.6 | 258.41 | 350.32 | 20.3450 |
| S1 | B | 248.7 | 38.21 | 376.97 | 3.3214 |
| | C | 144.8 | 12.89 | 287.64 | 3.3034 |
| | D | 53.4 | 7.28 | 175.64 | 3.1403 |
| | A | 286.5 | 150.50 | 392.36 | 17.8420 |
| S2 | B | 248.9 | 32.27 | 400.92 | 1.07530 |
| | C | 134.4 | 11.92 | 317.52 | 1.0890 |
| | D | 53.1 | 7.29 | 179.5 | 1.0703 |
| | A | 289.1 | 221.81 | 393.26 | 4.0421 |
| S3 | B | 262.8 | 41.37 | 419.69 | 1.1035 |
| | C | 158.9 | 13.74 | 305.39 | 1.2575 |
| | D | 55.7 | 7.43 | 175.93 | 0.7406 |
| | A | 289.5 | 230.90 | 306.9 | 41.2930 |
| S4 | B | 252.8 | 36.04 | 402.06 | 1.9992 |
| | C | 158.0 | 14.12 | 306.39 | 2.2050 |
| | D | 55.4 | 7.37 | 184.10 | 1.8893 |
| | A | 278.0 | 80.30 | 448.77 | 3.4598 |
| S5 | B | 218.9 | 22.45 | 332.31 | 2.8171 |
| | C | 126.5 | 11.31 | 256.61 | 2.7700 |
| | D | 49.1 | 7.00 | 160.47 | 2.4799 |
| | A | 264.3 | 81.22 | 361.36 | 13.9340 |
| S6 | B | 224.8 | 23.77 | 361.68 | 2.3431 |
| | C | 85.2 | 8.86 | 244.91 | 2.2601 |
| | D | 66.8 | 8.32 | 158.81 | 1.9419 |

Among all the AE descriptors, energy and average frequency are considered as the most important parameters than can reflect the physical mechanisms of the AE events. Energy is assumed to be proportional to the strain energy dissipated by the source of the fracture [14]. The frequency depends to a large extent on the properties of compositions involved in the micro-fracture process. Thus, cluster labelling can be proposed according to the energy and average frequency, combined with frequency domain analysis.

Fig.6 illustrates the energy and average frequency of the cluster centers of all six samples. Fig.7 shows the typical frequency spectra of the four classes of AE events collected from S3. It can be seen that the peak frequencies of Classes A to D are

350-380kHz, 320-340kHz, 270-290kHz, 240-260Hz, respectively. Classes A and B have a similar frequency domain, while their energies are quite different. This indicates that Classes A and B should belong to fracture of the same composition of C/SiC. Compared with the other two classes (C and D), Classes A and B, exhibiting the characteristics of higher frequency and higher energy, are associated with typical fiber breaking events [14]. Furthermore, since the energy of Class A is much higher than Class B, it can be inferred that Class A corresponds to the breaking events of fiber bundles, while Class B corresponds to the breaking events of single or a few fibers. Class D contains events with the lowest energy and frequency, which is consistent with the cracking of SiC matrix initiating at very low stress due to its brittle nature. Consequently, the remaining Class C may be labelled as interfacial damage.
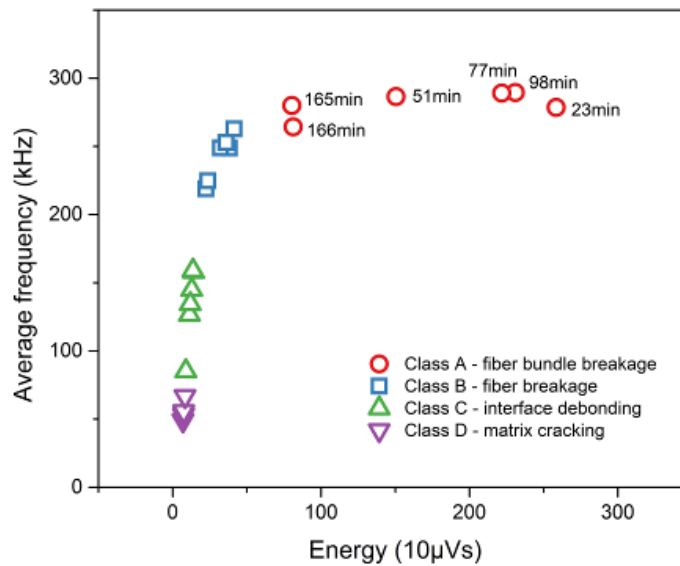


Fig. 6. Energy and average frequency of the four clusters of six samples.
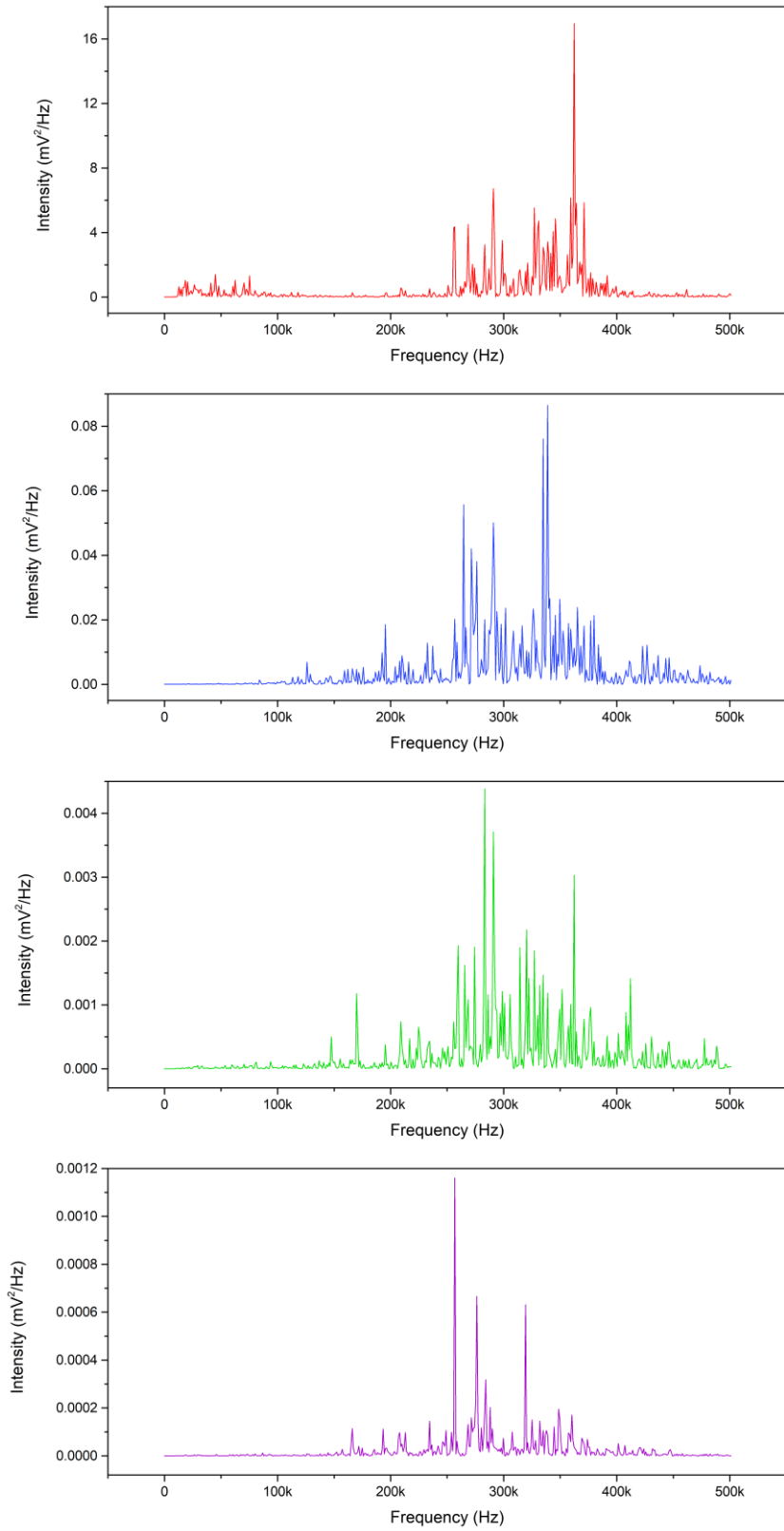
Fig. 7 Typical frequency spectra of the four classes of AE events collected from

S3.

Generally speaking, damage evolution within C/SiC includes the following processes: (a) a matrix crack initiates and propagates when C/SiC is loaded to a certain threshold stress; (b) with increasing stress, the matrix crack deflects and extends along the fiber-matrix interphase; (c) some weak fibers start to break and the matrix cracks propagates to the fiber-matrix interphase and deflects along the interphase. Thus, it is reasonable to posit that matrix cracking occurs earliest and fiber-bundle rupture occurs last. It is found from Table 2 that the first event of Class D and A occur earliest and last respectively, which conforms with the above cluster labelling results. The time of the first event for Classes B and C is very close.

*4.4 Damage evolution during stress rupture*

Once all the AE events are classified, the damage evolution during the whole creep lifetime can be described. The cumulative number and cumulative energy of various classes of AE events with creep time are shown in Fig.8 and Fig.9 respectively, in which the two samples with the shortest lifetime and the longest lifetime are compared. For other samples, the diagrams are similar. It can be seen from Fig.8 and Fig.9 that the evolution of Classes B, C, and D has an initial rapid accumulation period and a stable accumulation period until failure. Matrix cracking and interfacial damage are dominant and contribute more than 80% of the AE events. Although the AE events of fiber breakage are less than matrix cracking and interphase debonding, their cumulative energy is higher, indicating that failure of the fiber is the main energy dissipation process during creep. It seems that the numbers of AE events for matrix cracking and interfacial damage are the same for samples with various lives. On the

other hand, the numbers of AE events relevant to fiber failure are quite different, and the events of S1 are much fewer than those in S5.
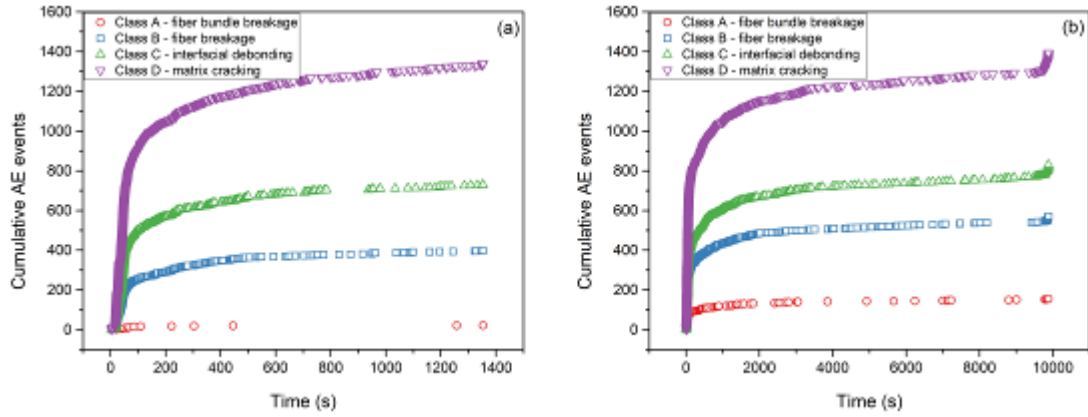


Fig. 8. The development of cumulative AE events with creep time (a) S1 and (b) S5.
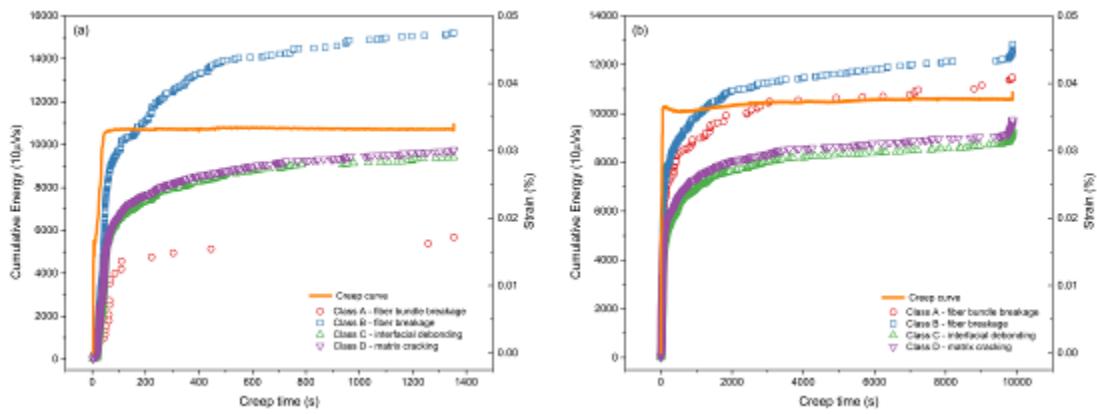


Fig. 9. The development of cumulative AE energy with creep time (a) S1 and (b) S5.

Stress rupture of C/SiC in a wet oxidizing atmosphere is a complex process coupling stress and oxidation effects. Generally speaking, stress produces cracks in coatings or the matrix and then promotes the diffusion of the oxidizing atmosphere, and the oxidation of carbon fibers reduces the load-carrying capacity. Due to this complexity, there may be different controlling damage mechanisms for different samples, depending on the nonuniformity of microscopic structures and flaws. Since the breakage of fiber-bundles is the most important factor affecting the mechanical properties, it is necessary to investigate the differences in the AE events labeled as

Class A in each sample, in order to interpret the controlling damage mechanisms

leading to different lifetimes.
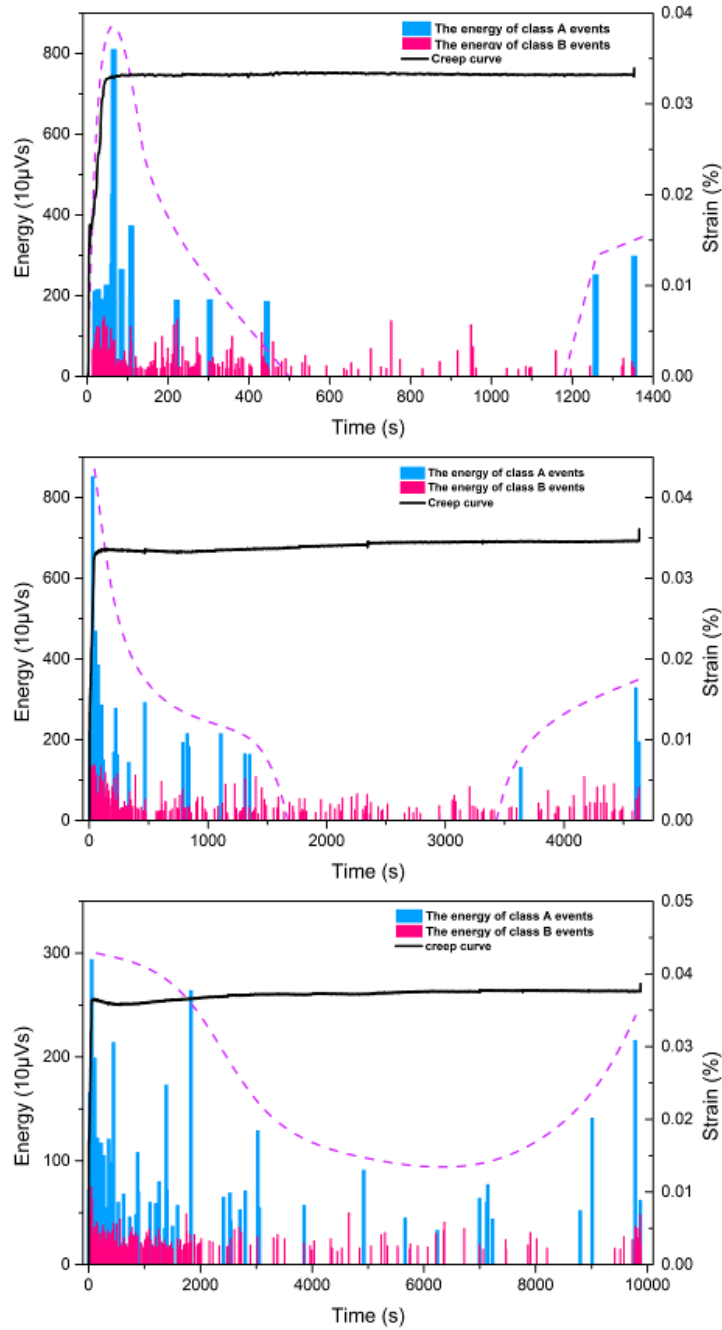


Fig.10. AE energy distribution of Class A and Class B for (a) S1, (b) S3 and (c) S5.

Fig. 10 illustrates the distribution of Class A events occurring during the test of S1,

S3 and S5. For S1 and S3, the events concentrate in the initial and final stages, and

there is a long period in the middle stage where no Class A events occur. For S5, there

are Class A events throughout the process. This phenomenon indicates that their controlling mechanisms are different. The first is termed a local damage mechanism, i.e., the dominant damage is produced in a local area, leading to stress concentration and rapid damage extension under stress until rupture occurs. The evidence for this is that there is an event with a much higher energy at the beginning. It is believed this unique event is released by a significant and substantial single breaking event. This AE event is the singule point in the PCA result identified earlier in Fig. 5. In this case, the rupture lifetime is shorter and the oxidation occurs in a local area. The second is termed a uniform damage mechanism, i.e., the oxidizing atmosphere diffuses uniformly and causes oxidation throughout. Then oxidized fiber bundles gradually break under the action of stress. In this case, the rupture lifetime is longer.

The above inference can also be proven by the following two considerations. One is the difference in the characteristics of Class A events of different samples, which depends on the pattern of the fiber bundles when they break. Another is the proportion of Class A events in all AE events, which can reflect the degree of concentration of fiber bundle failure.

It is found from Fig.6 that the cluster centers of B, C, and D classes are relatively less varied for all samples, while the average energies of Class A are distributed over a wide range. The AE energy of Class A is determined by the strain energy released when the fiber bundles break. In a wet oxidizing atmosphere, the fiber bundles may be oxidized to produce thinner fiber diameters, resulting in less release of strain energy when they break. Thus, it is believed that the difference in the AE energy of the six

samples is due to their different degree of oxidation. Fig.11 shows that the AE energy

of Class A decreases with increasing lifetime, indicating that the oxidation degree of

fibers in long-lived samples is more serious.
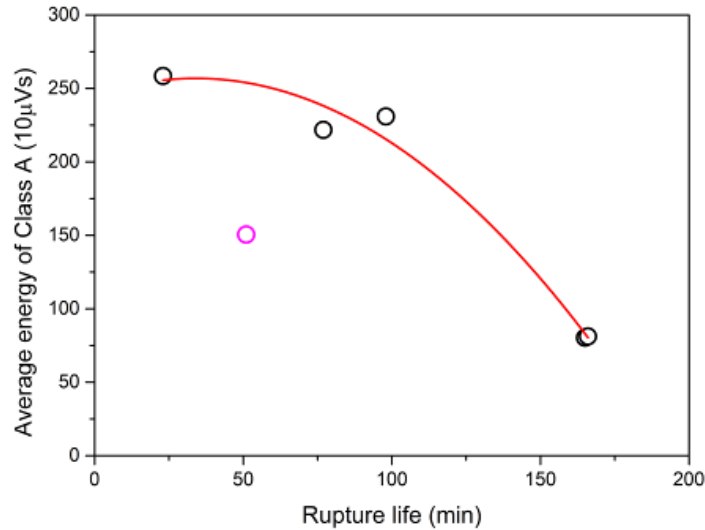


Fig.11. Relationship between the average energy of class A and the rupture lifetime.

Fig.12 shows the fracture morphologies of S1, S2, S3 and S5. For S1, owing to its

short lifetime, oxidizing gases have not yet diffused into the C/SiC. There has been

fiber oxidation only in a local area beneath the coating (Fig. 12(a)), while fibers in

most areas remain intact (Fig. 12(b)). The intact fiber bundles ensure that the AE

energy of Class A is very high. For S3, slight oxidation can be found within the

specimen (Fig. 12(e)) and some fibers in the oxidized area have separated from the

matrix and become thinner (Fig. 12(f)), resulting in an AE energy slight lower than

that of S1. Compared with S3, the shorter lifetime of S1 is due to the incomplete

deposition of SiC since there is a suspension point on it, which provides an original

source for rupture. For S5, even in the center of the specimen, oxidation can be found

(Fig.12(g)). Fibers in this region have become thinner and some of them have

completely disappeared (Fig.12(h)). The average AE energy of Class A is only about 30% of S1. In Fig.10, S2 is an exception. It has a very short lifetime but the AE energy of Class A is also quite low. It can be seen from Fig.12(c) that there is a large area of fiber pullout, which is difficult to find in other samples. The creep curve of S2 in Fig.2, with a high creep rate, also demonstrates the presence of fiber pullout. Fiber pullout means it is easier for the oxidizing atmosphere to contact and react with fibers. The sharp tips of broken fibers prove the truth of oxidation (Fig.12(d)). So, it is concluded that a weak fiber/matrix interphase is unfavorable for C/SiC under stress oxidation conditions.
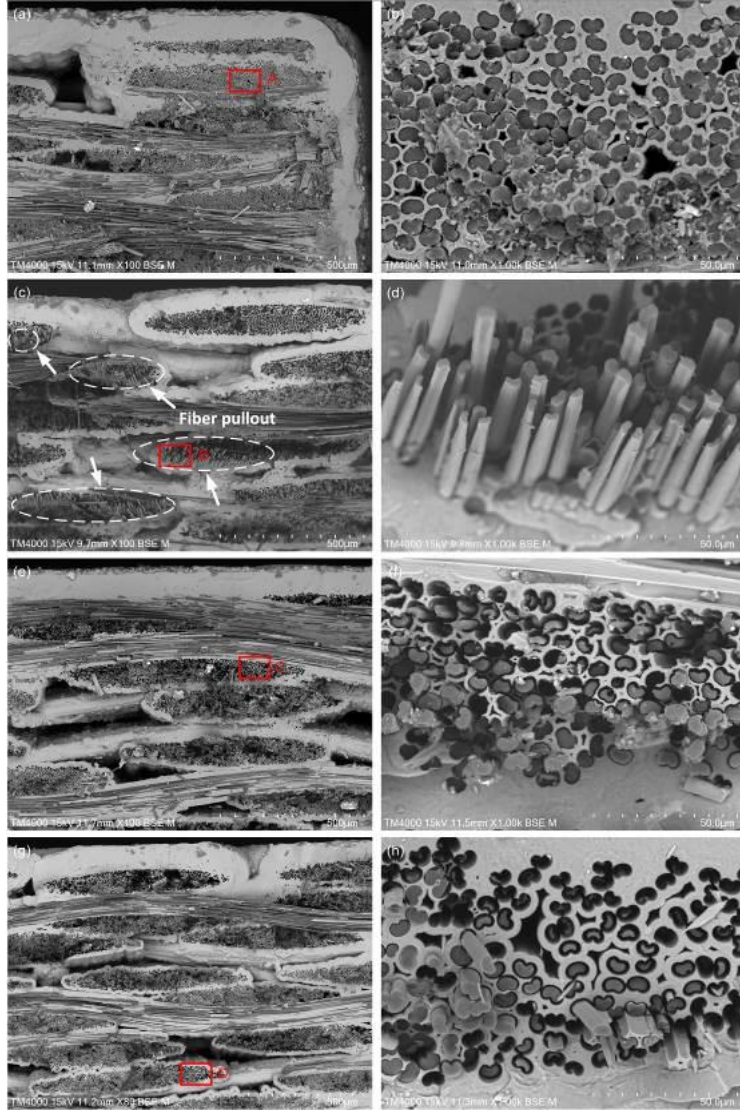
Fig.12. The SEM micrographs of the fracture surfaces: (a) S1, (b) enlarged view of area A, (c) S2, (d) enlarged view of area B, (e) S3, (f) enlarged view of area C, (g) S4, (h) enlarged view of area D.

One may define as the percentage of the total AE energy of the fiber-bundle breakage events to the total AE energy, and the percentage of the total AE events for fiber-bundle breakage to all AE events as:

$$F_{fb} = \frac{\sum_{i=1}^{n_{fb}} E_{fb}^{i}}{\sum_{j=1}^{n} E^{j}} \times 100\% \tag{4}$$

$$G_{fb} = \frac{n_{fb}}{n} \times 100\% \tag{5}$$

in which $n_{fb}$ is the number of fiber-bundle breakage events, $n$ is the total number of

AE events recorded, $E_{fb}^{i}$ is the energy of the $i$th event of fiber-bundle breakage, and

$E^{j}$ is the energy of the $j$th AE event.
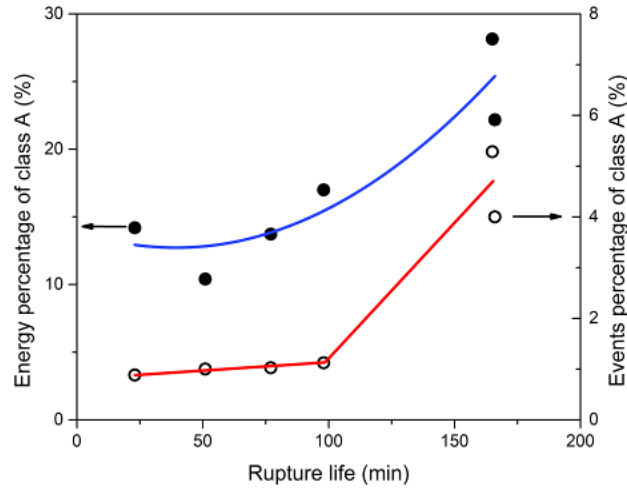


Fig.13. Variation of the energy and events percentage with rupture lifetime for Class

A.

Fig.13 illustrates the relationship of $F_{fb}$ and $G_{fb}$ against the rupture lifetime. It can

be seen that the $G_{fb}$ has two distinct regions. When the lifetime is less than 100min,

the percentage of Class A events has a slight increase with lifetime and the value is

only about 1%, indicating that fiber bundle breakage only occurs in some

concentrated area. Then there is a sharp rise when the lifetime becomes longer, due to

a transition to uniform damage mode. $F_{fb}$ shows a similar trend as $G_{fb}$, but the change

is more gradual.

**5. Conclusions**

Creep rupture lifetimes of C/SiC in a wet oxidizing atmosphere vary significantly.

AE was used find a correlation between failure mechanism and rupture lifetime. AE data collected during creep tests were divided into four clusters by an FCM algorithm, corresponding to the physical damage mechanisms of matrix cracking, interfacial damage, fiber breakage and fiber bundle breakage respectively. For samples with different lifetimes, the evolution of AE events and the AE features of fiber-bundle breakage are quite different. The percentage of cumulative AE energy corresponding to fiber bundle breakage has a relationship with rupture lifetime. The reason is hypothesized to be due to the extension and distribution of oxidation within C/SiC under different creep lifetime conditions. Local oxidation and damage development is the controlling failure mechanism for short-lived specimens and uniform oxidation and damage development is the controlling failure mechanism for long-lived specimens.

## Acknowledgements

## References

[1]  Naslain R. Design, preparation and properties of non-oxide CMCs for application in engines and nuclear reactors: an overview. Compos Sci Technol 2004; 64(2):155-170.

[2]  Schmidt S, Beyrer S, Knabe H, Immich H, Gessler A. Advanced ceramic matrix composite materials for current and future propulsion system applications. Acta

Astronaut 2004; 55(3-9):409-420.

[3] Verrilli MJ, Opila EJ, Calomino A, Kiser JD. Effect of environment on the stress-rupture behavior of a carbon-fiber-reinforced silicon carbide ceramic matrix composite. J Am Ceram Soc 2004; 87(8):1536-1542.

[4] Luan XG, Cheng LF, Zhang J, Li JZ, Zhang JT. Effects of temperature and stress on the oxidation behavior of a 3D C-SiC composite in a combustion wind tunnel. Compos Sci Technol, 2010; 70:678-684.

[5] Mei H. Modelling environmental effects on stress oxidation behaviour of carbon fibre reinforced ceramic matrix composites. Adv Appl Ceram 2009; 108(2):123-127.

[6] Liu YS, Zhang LT, Cheng LF, Yang WB. Effect of temperature on stress oxidation behaviors of 2D C/SiC-BCx composite in wet oxygen atmosphere. Metall Mater Trans A 2014; 45(2):5699-5707.

[7] Mansour R, Maillet E, Morscher GN. Monitoring interlaminar crack growth in ceramic matrix composites using electrical resistance. Script Mater 2015; 98:9-12.

[8] Smith CE, Morscher GN, Xia ZH. Electrical resistance as a nondestructive evaluation technique for sic/sic ceramic matrix composites under creep-rupture loading. Int J Appl Ceram Technol 2011; 8(2):298-307.

[9] Smith CE, Morscher GN, Xia ZH. Monitoring damage accumulation in ceramic matrix composites using electrical resistivity. Script Mater 2008; 59(4):463-466.

[10] Yang CP, Jiao GQ, Wang B, Huang T, Guo HB. Development of damage in a 2D

woven C/SiC composite under mechanical loading. Compos Part A 2015; 77:181-187.

[11] Li LB. Damage evolution of cross-ply ceramic-matrix composites under stress-rupture and cyclic loading at elevated temperatures in oxidizing atmosphere. Mater Sci Eng A 2017; 688: 315-321.

[12] Ruggles-Wrenn MB, Delapasse J, Chamberlain AL, Lane JE, Cook TS. Fatigue behavior of a Hi-Nicalon™/SiC–B4C composite at 1200 °C in air and in steam. Mater Sci Eng A 2012; 534:119-128.

[13] Li B, Tong XY, Yao LJ, Cheng QY. Infrared thermography for non-destructive evaluation of 2D C/Sic composites under fatigue loading. In: Proceedings of 3rd International Conference on Mechanical Engineering and Mechanics. Shengyang, September, 2009. p.296-300.

[14] Momon S, Godin N, Reynaud P, R'Mili M, Fantozzi G. Unsupervised and supervised classification of AE data collected during fatigue test on CMC at high temperature, Composites Part A 2012; 43(2):254-260.

[15] Momon S, Godin N, R'Mili M, Reynaud P, Fantozzi G, Fayolle G. Acoustic emission and lifetime prediction during static fatigue tests on ceramic-matrix-composite at high temperature under air. Compos Part A 2010; 41(7):913-918.

[16] Maillet E, Godin N, R'Mili M, Reynaud P, Lamon J, Fantozzi G. Analysis of acoustic emission energy release during static fatigue tests at intermediate temperatures on ceramic matrix composites: towards rupture time prediction.

Compos Sci Technol 2012; 72(9):1001-1007.

[17] Maillet E, Godin N, R'Mili M, Reynaud, Fantozzi G, Lamon J. Real-time evaluation of energy attenuation: a novel approach to acoustic emission analysis for damage monitoring of ceramic matrix composites. J Eur Ceram Soc 2014; 34(7):1673-1679.

[18] Maillet E, Godin N, R'Mili M, Reynaud, Fantozzi G. Fatigue lifetime of ceramic matrix composites at intermediate temperature by acoustic emission. Materials 2017; 10:658

[19] Wang JS, Yao LJ, Zhang L, Li B, Chen LD, Tong XY. Acoustic emission analysis on low velocity impact damage of 2D C/SiC composites. Adv Mater Res 2011; 301-303:1367-1371.

[20] Godin N, Reynaud P, Fantozzi G. Contribution of AE analysis in order to evaluate time to failure of ceramic matrix composites. Eng Fract Mech 2019; 210:452-469.

[21] Morscher GN, Maxwell R. Monitoring tensile fatigue crack growth and fiber failure around a notch in laminate SiC/SiC composites utilizing acoustic emission, electrical resistance, and digital image correlation. J Eur Ceram Soc 2019; 39(2-3):229-239.

[22] Morscher GN, Gordon NA. Acoustic emission and electrical resistance in SiC-based laminate ceramic composites tested under tensile loading. J Eur Ceram Soc 2017; 37(13):3861-3872.

[23] Li B, Tong XY, Feng ZY, Yao LJ. Infrared thermography and acoustic emission in 2D plain woven C/SiC composites under tensile-tensile fatigue loading. Adv

Mater Res 2010; 118-112:251-255.

[24] Liu CD, Cheng LF, Luan XG, Li B, Zhou J. Damage evolution and real-time non-destructive evaluation of 2D carbon-fiber/SiC-matrix composites under fatigue loading. Mater Lett 2008; 62(24):3922-3924.

[25] McCrory JP, Al-Jumaili SK, Crivelli D, Pearson MR, Eaton MJ, Featherston CA, Guagliano M, Holford KM, Pullin R. Damage classification in carbon fibre composites using acoustic emission: a comparison of three techniques. Compos Part B 2015; 68:424-430.

[26] Dahmene F, Yaacoubi S, Mountassir ME. Acoustic emission of composites structures: story, success, and challenges. Phys Procedia 2015; 70:599-603.

[27] Moevus M, Godin N, R'Mili M, Rouby D, Reynaud P, Fantozzi G, Farizy G. Analysis of damage mechanisms and associated acoustic emission in two SiC$_f$/[Si-B-C] composites exhibiting different tensile behaviours. Part II: unsupervised acoustic emission data clustering. Compos Sci Technol 2008; 68(6):1258-1265.

[28] Godin N, R'Mili M, Reynaud P, Fantozzi G, Lamon J. Identification of damage modes in ceramic matrix composites by acoustic emission signal pattern recognition. In: Ceram Eng Sci Proceedings 2011; 32(2):123-133.

[29] Wu SJ, Cheng LF, Zhang LT, Xu YD. Oxidation behavior of 2D C/SiC with a multi-layer CVD SiC coating. Surf Coat Technol 2006; 200(14-15):4489-4492.

[30] Mei H, Cheng LF, Luan XG, Zhang LT, Xu YD, Wang D. Simulated environments testing system for advanced ceramic matrix composites. Int J Appl

Ceram Technol 2006; 3(3):252-257.

[31]Liu CD, Cheng LF, Luan XG, Mei H, Wang CQ. Real-time damage evaluation of a SiC coated carbon/carbon composite under cyclic fatigue at high temperature in an oxidizing atmosphere. Mater Sci Eng A 2009; 524(1-2):98-101.

[32]Johnson M. Waveform based clustering and classification of AE transients in composite laminates using principal component analysis. NDT&E Int 2002; 35(6):367-376.

[33]Dunn JC. A fuzzy relative of the ISODATA process and its use in detecting compact well-separated clusters. J Cybernetics 1973; 3(3):32-57.

[34]Bezdek JC. Pattern recognition with fuzzy objective function algorithms. New York: Plenum Press, 1981.

[35]Chen SM, Chang YC. Multi-variable fuzzy forecasting based on fuzzy clustering and fuzzy rule interpolation techniques. Inform Sci 2010; 180(24):4772-4783.

[36]J.C. Bezdek, R. Ehrlich, W. Full. FCM: the fuzzy c-means clustering algorithm. Comp Geosci 1984; 10(2-3):191-203.

[37]Chaghari A, Feizi-Derakhshi M, Balafar M. Fuzzy clustering based on forest optimization algorithm. J King Saud Uni- Comp Inform Sci 2018; 30(1):25-32.

[38]Xie XL, Beni GA. Validity measure for fuzzy clustering. IEEE Trans Pattern Anal Mach Intell 1991; 13(8):841-846.

[39]Davies DL, Bouldin DW. A cluster separation measure. IEEE Trans Pattern Anal Mach Intell 1979; 1(2):224-227.